Nano Research
2021, 14(12): 4783–4788

ISSN 1998-0124 CN 11-5974/O4
https://doi.org/10.1007/s12274-021-3424-x

Research Article

NiCo-LDH nanosheets strongly coupled with GO-CNTs as a hybrid electrocatalyst for oxygen evolution reaction

Peiqun Yin[1,2,3] (✉), Geng Wu[2], Xiaoqian Wang[2], Shoujie Liu[5], Fangyao Zhou[2], Lei Dai[4] (✉), Xin Wang[2], Bo Yang[1], and Zhen-Qiang Yu[1] (✉)

[1] *School of Chemistry and Environmental Engineering, Institute of Low-dimensional Materials Genome Initiative, Shenzhen University, Shenzhen 518060, China*
[2] *School of Chemistry and Materials Science, Hefei National Laboratory for Physical Sciences at the Microscale, University of Science and Technology of China, Hefei 230026, China*
[3] *School of Biomedical Engineering and Research and Engineering Center of Biomedical Materials, Anhui Medical University, Hefei 230032, China*
[4] *Key Laboratory for Special Functional Materials of Ministry of Education, School of Materials, Henan University, Kaifeng 475004, China*
[5] *Chemistry and Chemical Engineering of Guangdong Laboratory, Shantou 515063, China*

Received: 29 January 2021 / **Revised:** 24 February 2021 / **Accepted:** 24 February 2021

ABSTRACT

The rational fabrication of highly efficient electrocatalysts with low cost toward oxygen evolution reaction (OER) is greatly desired but remains a formidable challenge. In this work, we present a facile and straightforward method of incorporating NiCo-layered double hydroxide (NiCo-LDH) into GO-dispersed CNTs (GO-CNTs) with interconnected configuration. X-ray absorption spectroscopy (XAS) reveals the strong electron interaction between NiCo-LDH and the underlying GO-CNTs substrate, which is supposed to facilitate charge transfer and accelerate the kinetics for OER. By tuning the amount of CNTs, the optimized NiCo-LDH/GO-CNTs composite can achieve a low overpotential of 290 mV at 10 mA·cm^{-2} current density, a small Tafel slope of 66.8 mV·dec^{-1} and robust stability, superior to the pure NiCo-LDH and commercial RuO_2 in alkaline media. The preeminent oxygen evolution performance is attributed to the synergistic effect stemming from the merits and the intimate electron interaction between LDH and GO-CNTs. This allows NiCo-LDH/GO-CNTs to be potentially applied in an industrial non-noble metal-based water electrolyzer as the anodic catalysts.

KEYWORDS

NiCo-LDH/GO-CNTs composite, electrocatalysts, oxygen evolution, intimate electron interaction

1 Introduction

Exploring sustainable energy resources and techniques to address the looming energy and environmental issues arising from the using of finite fossil fuel has become one of the most emergent task [1–6]. Several advanced electrochemical techniques including metal-air battery, water splitting and fuel cells, have been implemented for renewable and clean energy conversion and storage over the past few decades [7–12]. As a clean and sustainable energy source, hydrogen (H_2) is gradually changing the traditional energy conversion systems [13]. It should be noted that electrocatalytic water splitting has been considered as the most attractive and scalable strategy to generate clean H_2 at cathode (hydrogen evolution reaction (HER)) and O_2 at anode (oxygen evolution reaction (OER)) [14–16]. However, OER occurred at the anode side is regarded as the main bottleneck and uphill step in water splitting due to the multiple proton-coupled electron steps and kinetically sluggish process, which dramatically reduces the overall efficiency of water splitting [17–19]. Noble-metal electrocatalysts such as IrO_2 and RuO_2 are often used to drive OER. However, the prohibitively high cost and scarcity in nature of noble metals greatly restrict their commercial implementation. Therefore, it is highly desired to design and synthesize inexpensive and earth-abundant alternatives with superior activity and stability toward OER [20–22].

Recently, layered double hydroxides (LDHs) with two-dimensional (2D) hydrotalcite-like architectures have been considered as promising candidates for OER owing to their low cost, theoretically high activity, excellent stability, versatility in composition and facile preparation [23–26]. Thus, enormous efforts have been devoted to developing cost-effective LDHs with superior activities for OER [27–35]. However, the intrinsically inferior conductivity and the aggregation of LDHs are the two main problems that compromise their catalytic activity and kinetics during the electrochemical process. To address these issues, one promising approach is incorporating LDHs with electrically conductive carbon materials with high specific surface area, such as carbon nanotubes (CNTs), graphene or carbon quantum dots [36–41]. The resulted hybrids can increase the number of accessible active sites, and thus significantly improve OER performance. For instance, Dai et al. demonstrated that ultrathin NiFe-LDH nanoplates on mildly oxidized CNTs outperformed commercial Ir-based electrocatalysts in both

Address correspondence to Peiqun Yin, pqyin@mail.ustc.edu.cn; Lei Dai, dailei@henu.edu.cn; Zhen-Qiang Yu, zqyu@szu.edu.cn

activity and stability toward OER under alkaline conditions [40]. Qiao et al. fabricated a three-dimensional (3D) architecture hydrated catalyst by forming NiCo-LDH on N-doped graphene hydrogels, which expedite oxygen evolution because of the synergy of N-doped graphene and NiCo species [41]. Nevertheless, the chemical pre-treatment of CNTs or graphene was tedious and hazardous, which also destroyed the electronic structure of CNTs or graphene, leading to the deterioration of their intrinsic property.

Herein, we design a facile and straightforward strategy to load NiCo-LDH onto a carbon-based substrate, which used graphene oxide (GO) nanosheets (NSs) with oxygen functional groups as an amphiphilic surfactant to disperse pure CNTs (denoted as LDH/GO-*x*CNTs, wherein *x* represents the mass ratio between GO and CNTs). The preparation of LDH/GO-*x*CNT is schematically illustrated in Fig. 1(a) (see Experiment Section in the Electronic Supplementary Material (ESM) for details). We found that the optimal OER activity could be achieved when $x = 1$. The GO-CNTs, as the substrate to support NiCo-LDH are significant in several advantages: (1) the excellent water solubility of GO to disperse CNTs facilitates the contact between the electrocatalysts and the electrolyte, (2) the highly dispersed GO NSs and CNTs inhibit the aggregation of each other and thus increase the specific surface area, (3) the unfunctionalized CNTs provide high conductivity and enhance the electron transfer. Therefore, by providing a large surface area and high conductivity to NiCo-LDH, the resulting composite exhibits outstanding activity and superior stability toward OER ascribed to the synergistic effect originating from the merits and the intimate electron interaction between NiCo-LDH NSs and GO-CNTs.

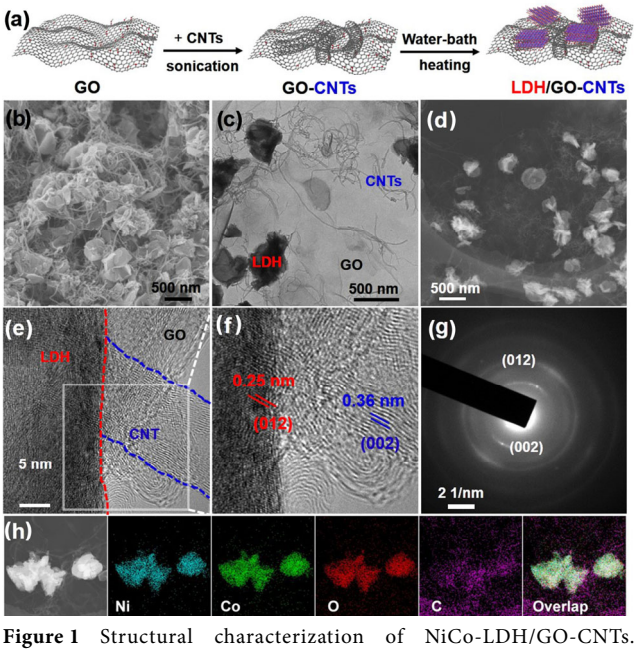

Figure 1 Structural characterization of NiCo-LDH/GO-CNTs. (a) Illustration of the synthesis procedure of NiCo-LDH/GO-CNTs composite. (b) SEM image, (c) TEM image and (d) HAADF-STEM image of NiCo-LDH/GO-CNTs. (e) HRTEM image. (f) The magnified part of the white solid square in (e). (g) The corresponding SAED pattern and (h) EDS elemental mapping of LDH/GO-CNTs.

2 Results and discussion

2.1 Physical characterization

The morphology and structure of GO, GO-CNTs and LDH/GO-CNTs were characterized by transmission electron microscopy (TEM) and scanning electron microscopy (SEM). The representative TEM images of GO (Fig. S1(a) in the ESM) and GO-CNTs (Fig. S1(b) in the ESM) suggest the successful adhesion of pristine CNTs onto the smooth surface of GO by mild sonication due to the π-π stacking interaction. Figure S2 in the ESM shows that GO-CNTs can generate a stable colloidal dispersion in water, while pristine CNTs is ineffective in contrast, confirming better dispersity. As shown in Fig. 1(b), NiCo-LDH NSs have successfully incorporated into the surface of GO-CNTs to form a 3D entangled network. TEM (Fig. 1(c)) and high-angle annular dark-field scanning transmission electron microscopy (HAADF-STEM) images (Fig. 1(d)) further validate the tight interconnection of ultrathin LDH, pristine CNTs and GO NSs. High-resolution TEM (HRTEM) (Figs. 1(e) and 1(f)) displays that two sets of interplanar distances of 0.25 and 0.36 nm, correspond to (012) plane of LDH NSs and (002) plane of graphitic carbon, respectively [35, 42]. The two diffraction rings in selected area electron diffraction (SAED) pattern (Fig. 1(g)) can be assigned to polycrystalline NiCo-LDH NSs and carbon, in good agreement with HRTEM. The corresponding elemental mapping (Fig. 1(h)) clearly demonstrates the homogeneous distribution of Ni, Co, O and C elements, which is consistent with X-ray energy dispersive spectroscopy (EDS) spectra (Fig. S3 in the ESM). All these results indicate the successful incorporation of NiCo-LDH NSs onto the GO-CNTs surface.

The crystal structures of the samples were examined by X-ray diffraction (XRD). The dominant diffraction peaks presented at 2θ values of about 12°, 24°, 35° and 60° can be indexed to (003), (006), (009) and (110) plane reflections, indicating the hydrotalcite-like LDH phase of the three samples (Fig. 2(a)) [43]. Notably, the diffraction peaks of carbon from GO-CNTs could not be observed in the XRD pattern for LDH/GO-CNTs, which may be attributed to the disordered stacking and uniform dispersion of GO and CNTs in the as-preformed composite [44]. Additionally, no peaks associated with byproducts such as oxides were detected, suggesting the high purity of the composites. X-ray photoelectron spectroscopy (XPS) further elucidates the chemical state of elements in the obtained samples. As shown in Fig. S4 in the ESM, the survey spectrum of LDH/GO-CNTs indicates the presence of Co, Ni, C, and O in

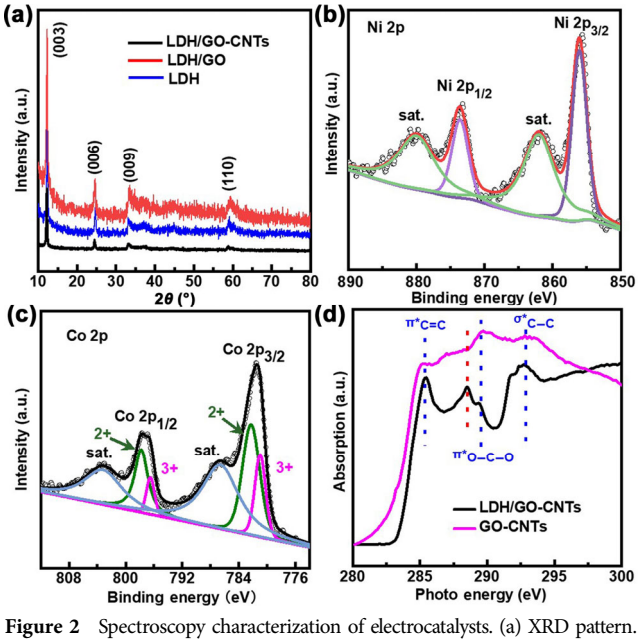

Figure 2 Spectroscopy characterization of electrocatalysts. (a) XRD pattern. (b) High resolution Ni 2p spectra for LDH/GO-CNTs. (c) High resolution Co 2p spectra for LDH/GO-CNTs. (d) C K-edge XANES spectra of LDH/GO-CNTs in comparision to GO-CNTs.

the composite. The C1s spectrum of GO-CNTs and LDH/GO-CNTs (Fig. S5 in the ESM) can be deconvoluted into four peaks, including O–C–O at 288.2 eV, C=O at 286.7 eV, C–O at 285.6 eV and C–C at 284.5 eV, proving the presence of hydrophilic functional groups [45]. In Ni 2p X-ray photoelectron spectroscopy (XPS) spectrum of the LDH/GO-CNTs composite (Fig. 2(b)), two obvious shakeup satellites (indicated as "sat.") close to two spin-orbit doublets at 873.2 and 855.6 eV can be identified as Ni $2p_{1/2}$ and $Ni2p_{3/2}$ signals of Ni^{2+} [46, 47]. The Co 2p XPS spectrum (Fig. 2(c)) can be fitted into two pairs of spin-orbit doublets including the peaks at 797.8 eV (Co $2p_{1/2}$) and 782.3 eV ($Co2p_{3/2}$) and the peaks at 796.5 eV ($Co2p_{1/2}$) and 781.0 eV ($Co2p_{3/2}$) accompanying with their corresponding shakeup satellites (indicated as "sat."), suggesting the co-existence of Co^{2+} and Co^{3+} in the composite [46, 48].

X-ray absorpotion spectroscopy (XAS) measurements were employed to give direct evidence of the electron interactions between NiCo-LDH and GO-CNTs and disclose in depth the local structure around Ni and Co atoms in the composite. As shown in the C K-edge absorption X-ray absorption near-edge structure (XANES) spectra, compared to the GO-CNTs alone, a prominent peak at ~ 288.5 eV is significantly aroused for the as-synthesized LDH/GO-CNTs composite (Fig. 2(d)), which can be assigned to the formation of M–O–C (M = Ni, Co) bonding originating from the carboxyl group (carbonyl π*), and thereby imply an obvious electron interaction between LDH NSs and GO-CNTs [40, 49, 50].

In addition, the Ni K-edge and the Co K-edge XANES spectra are shown in Figs. 3(a) and 3(b), respectively. The white-line peak intensity of LDH/GO-CNTs is obviously weakened as compared to that of the pure NiCo-LDH (Fig. 3(a)). Strikingly, the absorption edge position evaluated from the half height of the normalized edge jump of LDH/GO-CNTs in both Ni and Co K-edge XANES spectra shifts to lower energy (inset in Figs. 3(a) and 3(b)). Specifically, the energy downshift within the Ni K-edge XANES spectra between these two samples is more significant than that of Co, suggesting the much stronger impact of the carbon substrate (GO-CNTs) on Ni. These negative shifts certificate that the electronic structure around Ni and Co atoms is changed, probably due to the charge transfer from GO-CNTs to NiCo-LDH NSs, coinciding with the formation of M–O–C revealed by C K-edge absorption. More interestingly, LDH/GO-CNTs exhibits a higher pre-edge peak intensity than pure LDH in the Ni K-edge XANES (Fig. S6 in the ESM), implying a higher degree of octahedral geometry distortion at the Ni sites in LDH/GO-CNTs and this distortion should arise from the electron interaction between NiCo-LDH and GO-CNTs [29]. The Fourier transformed (FT) EXAFS curves at Ni K-edge and Co K-edge (Figs. 3(c) and 3(d)) provide more detailed information about the coordination environment at atomic level, respectively. The shape of FT curves does not change significantly besides a noticeable variation in the amplitude. The peak intensity of Ni K-edge EXAFS (Fig. 3(c)) spectrum for LDH/GO-CNTs obviously reduces compared with the pure LDH counterpart, which further indicates the structural distortion or dangling bonds around the Ni atoms, in line with the XANES analysis. The similar phenomenon was sighted on the Co K-edge EXAFS as well (Fig. 3(d)). To further elucidate the coordination information, the wavelet transform (WT) of the Ni and Co K-edge EXAFS were performed. Figures 3(e) and 3(f) display the WT contour plots of the Ni K-edge and Co K-edge, respectively. For both LDH/GO-CNTs and pure LDH, the signals from two WT maxima near 5.8 and 8 $Å^{-1}$ in Ni K-edge EXAFS WT analysis can be associated with Ni–O and Ni–Ni bond. Similarly, Co–O and Co–Co path are detected from the signals of 1.5 and 2.6 Å in Fig. 3(f). These results are coinciding with EXAFS analysis. The above investigations coherently confirm the intimate electron interaction and charge transfer between NiCo-LDH NSs and GO-CNTs, which are supposed to facilitate charge transport and accelerate the kinetics during OER, and further improve the OER performance.

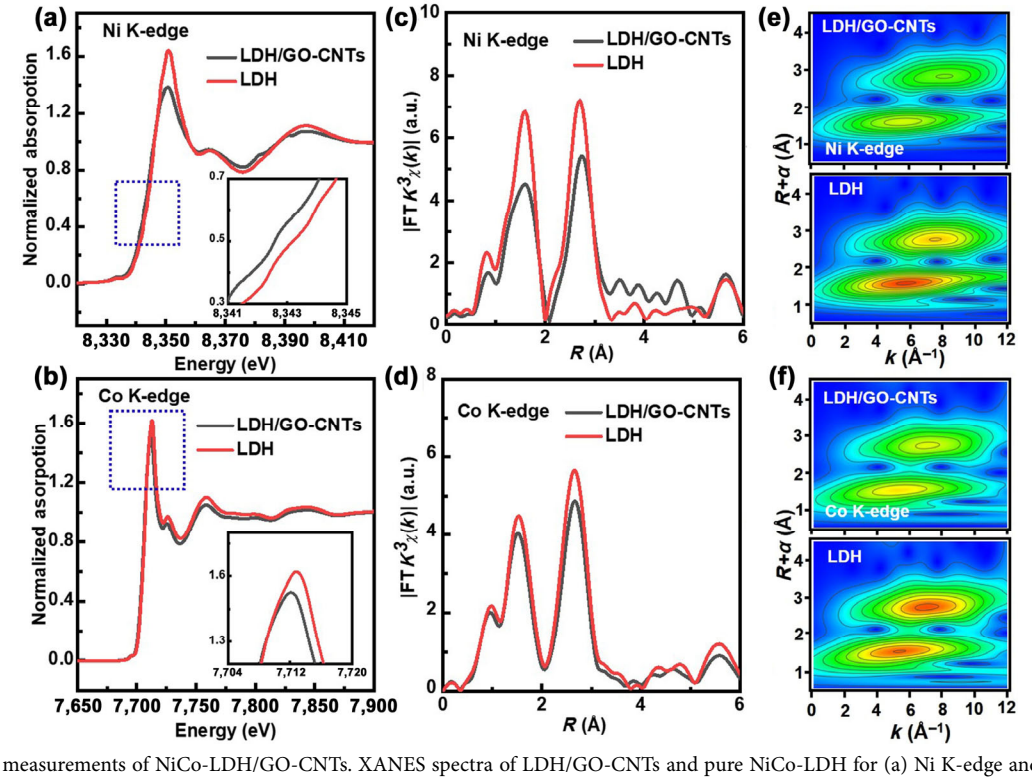

Figure 3 XAS measurements of NiCo-LDH/GO-CNTs. XANES spectra of LDH/GO-CNTs and pure NiCo-LDH for (a) Ni K-edge and (b) Co K-edge. Inset in ((a) and (b)): enlarged XANES spectrum taken from the blue dot square. FT EXAFS spectra of LDH/GO-CNTs and pure NiCo-LDH for (c) Ni K-edge and (d) Co K-edge. WT EXAFS spectra of LDH/GO-CNTs and pure NiCo-LDH for (e) Ni K-edge and (f) Co K-edge.

2.2 Electrocatalytic performance

The electrocatalytic OER activity of the synthesized catalysts was investigated by linear scan voltammetry (LSV) in O_2-saturated 0.1 M KOH solution with a standard three-electrode system. To optimize the activity of the composites, we prepared the composites with different mass ratio between GO and CNTs. As evidenced by LSV curves (Fig. S7 in the ESM), the best OER activity can be obtained when tune the mass ratio of GO and CNTs to 1. For comparison, Fig. 4(a) displays the LSV curves for OER over the synthesized electrocatalysts in alkaline media. Among them, the current density of LDH/GO-CNTs across the whole potential region is significantly superior to those of the other electrocatalysts. Additionally, LDH/GO-CNTs displays the smallest onset potential of 1.43 V vs. RHE and requires an overpotential of 260 mV to afford a current density of 5 mA·cm^{-2}, lower than those of GO-LDH (410 mV), bare LDH (390 mV) and GO-CNTs (400 mV) (Fig. 4(b)). More importantly, LDH/GO-CNTs composite affords 10 mA·cm^{-2} at a small overpotential of 290 mV, even lower than those of commercial RuO_2 (320 mV) and other reported non-noble metal-based electrocatalysts, which is shown in Table S1 in the ESM [48, 49, 51–54]. Such a low overpotential and high current density underscore that LDH/GO-CNTs is a highly active OER catalysts. As Tafel slope is a key factor to evaluate the OER kinetics, the smaller Tafel slope down to 66.8 mV·dec^{-1} compared to those of LDH/GO (139.0 mV·dec^{-1}), LDH (132.9 mV·dec^{-1}) and GO-CNTs (82.9 mV·dec^{-1}) demonstrates its more favorable reaction kinetics, which is shown in Fig. 4(c). To further certify better OER electrocatalytic efficiency for LDH/GO-CNTs, electrochemical impedance spectroscopy (EIS) was conducted to investigate the electrode kinetics under OER condition. The Nyquist plots and the enlarged Nyquist plots in the high frequency region (Fig. S8 and the inset) reveal that the resolution resistance (R_s) and charge-transfer resistance (R_{ct}) of the LDH/GO-CNTs show an obvious decrease in comparison with other electrocatalysts. This evidence suggests that LDH/GO-CNTs possesses the fastest charge transfer process among these catalysts, which could be ascribed to the intimate electron interaction between NiCo-LDH NSs and GO-CNTs.

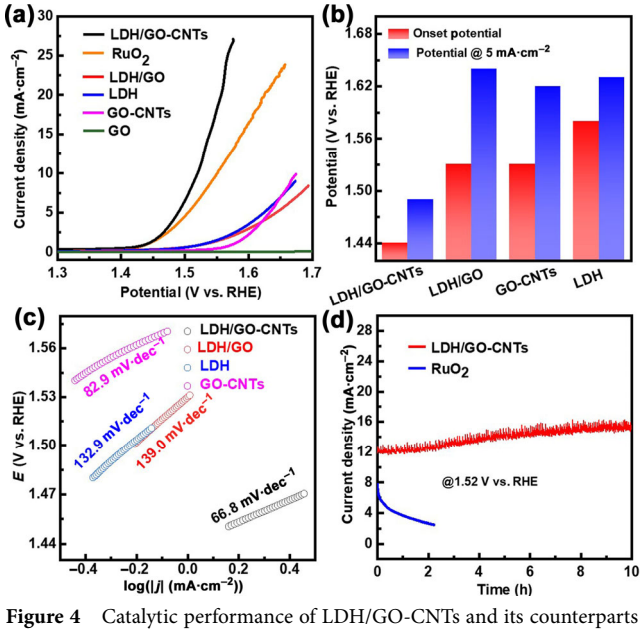

Figure 4 Catalytic performance of LDH/GO-CNTs and its counterparts for OER. (a) Electrode surface area-normalized polarization curves in 0.1 M KOH aqueous solution. (b) The potentials required for onset and a current density of 5 mA·cm^{-2}. (c) Corresponding Tafel plots obtained from (a). (d) Chronoamperometric curve of LDH/GO-CNTs and commercial RuO_2 at 1.52 V (vs. RHE) for 10 and 2 h, respectively.

Despite high activity, durability is another critical parameter to assess the performance of electrocatalysts. As shown in Fig. 4(d), the time-dependent current density for LDH/GO-CNTs at 1.52 V (vs. RHE) shows a little increase rather than degradation within 10 h. In contrast, the current density of commercial RuO_2 drops by 75% within 2 h of catalyzing, which is inferior to our electrocatalyst. The increase in the current density with time is mainly because the catalyst surface is further activated during the electrocatalytic process [55–57]. This indicates that LDH/GO-CNTs has the potential to become an excellent catalyst for OER. Likewise, the polarization curve for LDH/GO-CNTs after 1,000 continuous potential cycles displays insignificant change in the current density (Fig. S9 in the ESM). The tested composite was then subjected to TEM characterization including HRTEM (Fig. S10 in the ESM), elemental mapping (Fig. S11 in the ESM) and SAED (Fig. S12 in the ESM), manisfesting that the structure of NiCo-LDH/GO-CNTs is still preserved after the catalytic process. This highlights the outstanding structural robustness of LDH/GO-CNTs under long-term durability test.

3 Conclusion

In summary, we have successfully developed a straightforward and facile strategy to directly grow NiCo-LDH onto GO-CNTs. The NiCo-LDH/GO-CNTs possesses excellent OER activity and superior stability, making it a promising OER electrocatalysts for future implementation. We believe that the unparalleled OER performances of the composites are attributed to the synergistic effect originating from the advantages and the intimate electron interaction between LDH and GO-CNTs, which provides accessible active sites and enables fast charge transport during OER. The NiCo-LDH are the active sites of oxygen evolution reaction, and the GO-CNTs plays the roles of carrier and promotor. Taking accounts of the simplicity of our strategy and the excellent OER performance, this work provides new insights in the rational design and synthesis of low cost and highly efficient catalysts for sustainable electrochemical energy conversion.

Acknowledgements

This work was supported by Science and Technology Key Project of Guangdong Province of China (No. 2020B010188002), the National Major Science and Technology Program for Water Pollution Control and Treatment of China (No. 2017ZX07202). We sincerely thank the photoemission endstations beamline 1W1B station in Beijing Synchrotron Radiation Facility (BSRF), BL10B and BL11U in National Synchrotron Radiation Laboratory (NSRL) in Hefei, China.

Electronic Supplementary Material: Supplementary material (further details of the experimental section, SEM/TEM images, SAED pattern, XPS spectra, XANES spectra, electrochemical performance, EIS characterization and so on) is available in the online version of this article at https://doi.org/10.1007/s12274-021-3424-x.

References

[1] Yang, Z. G.; Zhang, J. L.; Kintner-Meyer, M. C. W.; Lu, X. C.; Choi, D.; Lemmon, J. P.; Liu, J. Electrochemical energy storage for green grid. *Chem. Rev.* **2011**, *111*, 3577–3613.
[2] Chu, S.; Majumdar, A. Opportunities and challenges for a sustainable energy future. *Nature* **2012**, *488*, 294–303.
[3] Chen, J. G.; Crooks, R. M.; Seefeldt, L. C.; Bren, K. L.; Bullock, R.

M.; Darensbourg, M. Y.; Holland, P. L.; Hoffman, B.; Janik, M. J.; Jones, A. K. et al. Beyond fossil fuel-driven nitrogen transformations. *Science* **2018**, *360*, eaar6611.

[4] Li, X. N.; Liu, L. H.; Ren, X. Y.; Gao, J. J.; Huang, Y. Q.; Liu, B. Microenvironment modulation of single-atom catalysts and their roles in electrochemical energy conversion. *Sci. Adv.* **2020**, *6*, eabb6833.

[5] Liu, H. L.; Zhu, Y. T.; Ma, J. M.; Zhang, Z. C.; Hu, W. P. Recent advances in atomic-level engineering of nanostructured catalysts for electrochemical CO_2 reduction. *Adv. Funct. Mater.* **2020**, *30*, 1910534.

[6] Qin, Q.; Oschatz, M. Overcoming chemical inertness under ambient conditions: A critical view on recent developments in ammonia synthesis via electrochemical N_2 reduction by asking five questions. *ChemElectroChem* **2020**, *7*, 878–889.

[7] Mistry, H.; Varela, A. S.; Kühl, S.; Strasser, P.; Cuenya, B. R. Nanostructured electrocatalysts with tunable activity and selectivity. *Nat. Rev. Mater.* **2016**, *1*, 16009.

[8] Seh, Z. W.; Kibsgaard, J.; Dickens, C. F.; Chorkendorff, I.; Nørskov, J. K.; Jaramillo, T. F. Combining theory and experiment in electrocatalysis: Insights into materials design. *Science* **2017**, *355*, eaad4998.

[9] Wang, H. F.; Xu, Q. Materials design for rechargeable metal-air batteries. *Matter* **2019**, *1*, 565–595.

[10] Dai, L. M.; Xue, Y. H.; Qu, L. T.; Choi, H. J.; Baek, J. B. Metal-free catalysts for oxygen reduction reaction. *Chem. Rev.* **2015**, *115*, 4823–4892.

[11] Yin, P. Q.; You, B. Atom migration-trapping toward single-atom catalysts for energy electrocatalysis. *Mater. Today Energy* **2021**, *19*, 100586.

[12] Yin, P. Q.; Yao, T.; Wu, Y.; Zheng, L. R.; Lin, Y.; Liu, W.; Ju, H. X.; Zhu, J. F.; Hong, X.; Deng, Z. X. et al. Single cobalt atoms with precise N-coordination as superior oxygen reduction reaction catalysts. *Angew. Chem., Int. Ed.* **2016**, *55*, 10800–10805.

[13] Bockris, J. O. M. The origin of ideas on a hydrogen economy and its solution to the decay of the environment. *Int. J. Hydrog. Energy* **2002**, *27*, 731–740.

[14] Gao, M. R.; Zheng, Y. R.; Jiang, J.; Yu, S. H. Pyrite-type nanomaterials for advanced electrocatalysis. *Acc. Chem. Res.* **2017**, *50*, 2194–2204.

[15] Roger, I.; Shipman, M. A.; Symes, M. D. Earth-abundant catalysts for electrochemical and photoelectrochemical water splitting. *Nat. Rev. Chem.* **2017**, *1*, 0003.

[16] You, B.; Sun, Y. J. Innovative strategies for electrocatalytic water splitting. *Acc. Chem. Res.* **2018**, *51*, 1571–1580.

[17] Jiao, Y.; Zheng, Y.; Jaroniec, M.; Qiao, S. Z. Design of electrocatalysts for oxygen- and hydrogen-involving energy conversion reactions. *Chem. Soc. Rev.* **2015**, *44*, 2060–2086.

[18] Yao, Y. C.; Hu, S. L.; Chen, W. X.; Huang, Z. Q.; Wei, W. C.; Yao, T.; Liu, R. R.; Zang, K. T.; Wang, X. Q.; Wu, G. et al. Engineering the electronic structure of single atom Ru sites via compressive strain boosts acidic water oxidation electrocatalysis. *Nat. Catal.* **2019**, *2*, 304–313.

[19] Song, J. J.; Wei, C.; Huang, Z. F.; Liu, C. T.; Zeng, L.; Wang, X.; Xu, Z. J. A review on fundamentals for designing oxygen evolution electrocatalysts. *Chem. Soc. Rev.* **2020**, *49*, 2196–2214.

[20] Dai, L.; Chen, Z. N.; Li, L. X.; Yin, P. Q.; Liu, Z. Q.; Zhang, H. Ultrathin Ni(0)-embedded $Ni(OH)_2$ heterostructured nanosheets with enhanced electrochemical overall water splitting. *Adv. Mater.* **2020**, *32*, 1906915.

[21] Hong, W. T.; Risch, M.; Stoerzinger, K. A.; Grimaud, A.; Suntivich, J.; Shao-Horn, Y. Toward the rational design of non-precious transition metal oxides for oxygen electrocatalysis. *Energy Environ. Sci.* **2015**, *8*, 1404–1427.

[22] Wang, H. F.; Chen, L. Y.; Pang, H.; Kaskel, S.; Xu, Q. MOF-derived electrocatalysts for oxygen reduction, oxygen evolution and hydrogen evolution reactions. *Chem. Soc. Rev.* **2020**, *49*, 1414–1448.

[23] Wang, Q.; O'Hare, D. Recent advances in the synthesis and application of layered double hydroxide (LDH) nanosheets. *Chem. Rev.* **2012**, *112*, 4124–4155.

[24] Fan, G. L.; Li, F.; Evans, D. G.; Duan, X. Catalytic applications of layered double hydroxides: recent advances and perspectives. *Chem. Soc. Rev.* **2014**, *43*, 7040–7066.

[25] Laipan, M. W.; Yu, J. F.; Zhu, R. L.; Zhu, J. X.; Smith, A. T.; He, H. P.; O'Hare, D.; Sun, L. Y. Functionalized layered double hydroxides for innovative applications. *Mater. Horiz.* **2020**, *7*, 715–745.

[26] Hu, T. T.; Mei, X.; Wang, Y. J.; Weng, X. S.; Liang, R. Z.; Wei, M. Two-dimensional nanomaterials: fascinating materials in biomedical field. *Sci. Bull.* **2019**, *64*, 1707–1727.

[27] Xie, Q. X.; Cai, Z.; Li, P. S.; Zhou, D. J.; Bi, Y. M.; Xiong, X. Y.; Hu, E. Y.; Li, Y. P.; Kuang, Y.; Sun, X. M. Layered double hydroxides with atomic-scale defects for superior electrocatalysis. *Nano Res.* **2018**, *11*, 4524–4534.

[28] Song, F.; Hu, X. L. Ultrathin cobalt-manganese layered double hydroxide is an efficient oxygen evolution catalyst. *J. Am. Chem. Soc.* **2014**, *136*, 16481–16484.

[29] Wang, D. W.; Li, Q.; Han, C.; Lu, Q. Q.; Xing, Z. C.; Yang, X. R. Atomic and electronic modulation of self-supported nickel-vanadium layered double hydroxide to accelerate water splitting kinetics. *Nat. Commun.* **2019**, *10*, 3899.

[30] Song, F.; Hu, X. L. Exfoliation of layered double hydroxides for enhanced oxygen evolution catalysis. *Nat. Commun.* **2014**, *5*, 4477.

[31] Liang, H. F.; Meng, F.; Cabán-Acevedo, M.; Li, L. S.; Forticaux, A.; Xiu, L. C.; Wang, Z. C.; Jin, S. Hydrothermal continuous flow synthesis and exfoliation of NiCo layered double hydroxide nanosheets for enhanced oxygen evolution catalysis. *Nano Lett.* **2015**, *15*, 1421–1427.

[32] Zhou, D. J.; Wang, S. Y.; Jia, Y.; Xiong, X. Y.; Yang, H. B.; Liu, S.; Tang, J. L.; Zhang, J. M.; Liu, D.; Zheng, L. R. et al. NiFe hydroxide lattice tensile strain: Enhancement of adsorption of oxygenated intermediates for efficient water oxidation catalysis. *Angew. Chem., Int. Ed.* **2019**, *58*, 736–740.

[33] Zheng, Z. M.; Lin, L. L.; Mo, S. G.; Ou, D. H.; Tao, J.; Qin, R. X.; Fang, X. L.; Zheng, N. F. Economizing production of diverse 2D layered metal hydroxides for efficient overall water splitting. *Small* **2018**, *14*, 1800759.

[34] Zou, X. X.; Goswami, A.; Asefa, T. Efficient noble metal-free (electro)catalysis of water and alcohol oxidations by zinc-cobalt layered double hydroxide. *J. Am. Chem. Soc.* **2013**, *135*, 17242–17245.

[35] Sirisomboonchai, S.; Li, S. S.; Yoshida, A.; Li, X. M.; Samart, C.; Abudula, A.; Guan, G. Q. Fabrication of NiO microflake@NiFe-LDH nanosheet heterostructure electrocatalysts for oxygen evolution reaction. *ACS Sustainable Chem. Eng.* **2019**, *7*, 2327–2334.

[36] Long, X.; Li, J. K.; Xiao, S.; Yan, K. Y.; Wang, Z. L.; Chen, H. N.; Yang, S. H. A strongly coupled graphene and FeNi double hydroxide hybrid as an excellent electrocatalyst for the oxygen evolution reaction. *Angew. Chem., Int. Ed.* **2014**, *53*, 7584–7588.

[37] Tang, C.; Wang, H. S.; Wang, H. F.; Zhang, Q.; Tian, G. L.; Nie, J. Q.; Wei, F. Spatially confined hybridization of nanometer-sized NiFe hydroxides into nitrogen-doped graphene frameworks leading to superior oxygen evolution reactivity. *Adv. Mater.* **2015**, *27*, 4516–4522.

[38] Ma, W.; Ma, R. Z.; Wang, C. X.; Liang, J. B.; Liu, X. H.; Zhou, K. C.; Sasaki, T. A superlattice of alternately stacked Ni-Fe hydroxide nanosheets and graphene for efficient splitting of water. *ACS Nano* **2015**, *9*, 1977–1984.

[39] Tang, D.; Liu, J.; Wu, X. Y.; Liu, R. H.; Han, X.; Han, Y. Z.; Huang, H.; Liu, Y.; Kang, Z. H. Carbon quantum dot/NiFe layered double-hydroxide composite as a highly efficient electrocatalyst for water oxidation. *ACS Appl. Mater. Interfaces.* **2014**, *6*, 7918–7925.

[40] Gong, M.; Li, Y. G.; Wang, H. L.; Liang, Y. Y.; Wu, J. Z.; Zhou, J. G.; Wang, J.; Regier, T.; Wei, F.; Dai, H. J. An advanced Ni-Fe layered double hydroxide electrocatalyst for water oxidation. *J. Am. Chem. Soc.* **2013**, *135*, 8452–8455.

[41] Chen, S.; Duan, J. J.; Jaroniec, M.; Qiao, S. Z. Three-dimensional N-doped graphene hydrogel/NiCo double hydroxide electrocatalysts for highly efficient oxygen evolution. *Angew. Chem., Int. Ed.* **2013**, *52*, 13567–13570.

[42] Zhang, M.; Zhang, J. T.; Ran, S. Y.; Qiu, L. X.; Sun, W.; Yu, Y.; Chen, J. S.; Zhu, Z. H. A robust bifunctional catalyst for rechargeable Zn-air batteries: Ultrathin NiFe-LDH nanowalls vertically anchored on soybean-derived Fe-N-C matrix. *Nano Res.* **2021**, *14*, 1175–1186.

[43] Wang, T. J.; Liu, X. Y.; Li, Y.; Li, F. M.; Deng, Z. W.; Chen, Y. Ultrasonication-assisted and gram-scale synthesis of Co-LDH nanosheet aggregates for oxygen evolution reaction. *Nano Res.* **2020**, *13*, 79–85.

[44] Yan, J.; Fan, Z. J.; Sun, W.; Ning, G. Q.; Wei, T.; Zhang, Q.; Zhang, R. F.; Zhi, L. J.; Wei, F. Advanced asymmetric supercapacitors based on

$Ni(OH)_2$/graphene and porous graphene electrodes with high energy density. *Adv*. *Funct*. *Mater*. **2012**, *22*, 2632–2641.

[45] Musielak, M.; Gagor, A.; Zawisza, B.; Talik, E.; Sitko, R. Graphene oxide/carbon nanotube membranes for highly efficient removal of metal ions from water. *ACS Appl*. *Mater*. *Interfaces* **2019**, *11*, 28582–28590.

[46] Zhu, L. L.; Hao, C.; Wang, X. H.; Guo, Y. N. Fluffy cotton-like GO/Zn-Co-Ni layered double hydroxides form from a sacrificed template GO/ZIF-8 for high performance asymmetric supercapacitors. *ACS Sustainable Chem*. *Eng*. **2020**, *8*, 11618–11629.

[47] Chen, H.; Hu, L. F.; Chen, M.; Yan, Y.; Wu, L. M. Nickel-cobalt layered double hydroxide nanosheets for high-performance supercapacitor electrode materials. *Adv*. *Funct*. *Mater*. **2014**, *24*, 934–942.

[48] Ma, T. Y.; Dai, S.; Jaroniec, M.; Qiao, S. Z. Metal-organic framework derived hybrid Co_3O_4-carbon porous nanowire arrays as reversible oxygen evolution electrodes. *J*. *Am*. *Chem*. *Soc*. **2014**, *136,* 13925–13931.

[49] Leng, M.; Huang, X. L.; Xiao, W.; Ding, J.; Liu, B. H.; Du, Y. H.; Xue, J. M. Enhanced oxygen evolution reaction by Co-O-C bonds in rationally designed Co_3O_4/graphene nanocomposites. *Nano Energy* **2017**, *33*, 445–452.

[50] Liu, H. J.; Zhou, J.; Wu, C. Q.; Wang, C. D.; Zhang, Y. K.; Liu, D. B.; Lin, Y. X.; Jiang, H. L.; Song, L. Integrated flexible electrode for oxygen evolution reaction: Layered double hydroxide coupled with single-walled carbon nanotubes Film. *ACS Sustainable Chem*. *Eng*. **2018**, *6*, 2911–2915.

[51] Gao, M. R.; Sheng, W. C.; Zhuang, Z. B.; Fang, Q. R.; Gu, S.; Jiang, J.; Yan, Y. S. Efficient water oxidation using nanostructured α-Nickel-hydroxide as an electrocatalyst. *J*. *Am*. *Chem*. *Soc*. **2014**, *136*, 7077–7084.

[52] Zhou, D. J.; Cai, Z.; Bi, Y. M.; Tian, W. L.; Luo, M.; Zhang, Q.; Zhang, Q.; Xie, Q. X.; Wang, J. D.; Li, Y. P. et al. Effects of redox- active interlayer anions on the oxygen evolution reactivity of NiFe- layered double hydroxide nanosheets. *Nano Res*. **2018**, *11*, 1358–1368.

[53] Zhao, A. Q.; Masa, J.; Xia, W.; Maljusch, A.; Willinger, M. G.; Clavel, G.; Xie, K. P.; Schlögl, R.; Schuhmann, W.; Muhler, M. Spinel Mn-Co oxide in N-doped carbon nanotubes as a bifunctional electrocatalyst synthesized by oxidative cutting. *J*. *Am*. *Chem*. *Soc*. **2014**, *136*, 7551–7554.

[54] Ding, D. N.; Shen, K.; Chen, X. D.; Chen, H. R.; Chen, J. Y.; Fan, T.; Wu, R. F.; Li, Y. W. Multi-level architecture optimization of MOF-templated Co-based nanoparticles embedded in hollow N‐Doped carbon polyhedra for efficient OER and ORR. *ACS Catal*. **2018**, *8*, 7879–7888.

[55] Dai, L.; Qin, Q.; Zhao, X. J.; Xu, C. F.; Hu, C. Y.; Mo, S. G.; Wang, Y. O.; Lin, S. C.; Tang, Z. C.; Zheng, N. F. Electrochemical partial reforming of ethanol into ethyl acetate using ultrathin Co_3O_4 nanosheets as a highly selective anode catalyst. *ACS Cent*. *Sci*. **2016**, *2*, 538–544.

[56] Joo. J.; Kim, T.; Lee, J.; Choi, S. I.; Lee, K. Morphology-controlled metal sulfides and phosphides for electrochemical water splitting. *Adv*. *Mater*. **2019**, *31*, 1806682.

[57] Wang, H. Y.; Hsu, Y. Y.; Chen, R.; Chan, T. S.; Chen, H. M.; Liu, B. Ni^{3+}-induced formation of active NiOOH on the spinel Ni-Co oxide surface for efficient oxygen evolution reaction. *Adv*. *Energy Mater*. **2015**, *5*, 1500091.